A climatic control on reorganization of ocean circulation during the n1id-Cenomanian Event and Cenomanian-Turonian oceanic anoxic event (OAE-2): Nd-isotope evidence

Xin-Yuan Zheng[1]*, Hugh C. Jenkyns[1], Andrew S. Gale\ David J. Ward3, and Gideon M. Henderson[1]

[1]*Department of Earth Sciences, University of Oxford, South Parks Road, O;iford OXJ 3AN, UK*

[2]*School of Earth and Environmental Sciences, University of Portsmouth, Burnaby Road, Portsmouth POI 3QL, UK*

[3]*Department of Earth Sciences, The Natural History Museum, Cromwell Road, London SW7 5BD, UK*

*Cunent address: Department of Geoscience, University of Wisconsin-Madison, WI 53706, USA. E-mail: xzheng75@wisc.edu.

ABSTRACT

Although ocean circulation plays an essential role in the climate system, its response to major carbon-cycle perturbations during the mid-Cretaceous, including the Mid-Cenomanian Event I (MCE I) and Cenomanian-Turonian oceanic anoxic event (OAE 2), is poorly constrained. Here we present Nd-isotope evidence for episodic increases in the influence of boreal seawater in the European epicontinental Chalk Sea during MCE I. The start of this reorganization of circulation lagged the onset of the $\delta^{13}C$ positive excursion defining MCE I. This sequence of change is similar to that observed during OAE 2 in the same area, showing a consistent response of circulation to changes in the global carbon cycle. Brief intervals of southerly spread of boreal fauna into mid-latitudinal seas, two during MCE I and one during OAE 2 (Plenus Cold Event), always started after the influence of boreal seawater was enhanced, implying a slower biological response to climatic cooling, rather than passive transport of fauna by boreal waters. The lack of an Nd-isotope positive excursion in our record across MCE I supports a volcanic origin for prominent increases in seawater Nd-isotope values found in the European epicontinental Chalk Sea and tropical Atlantic sequences during OAE 2. The observed tight circulation-carbon cycle coupling potentially serves as an important route for replenishing upper-ocean nutrients from deep waters and/or volcanic sources, providing a critical feedback allowing continuation of MCE I and OAE 2 over considerable time periods.

INTRODUCTION

The mid-Cenomanian event I (MCE I, 96 Ma) and Cenomanian-Turonian oceanic anoxic event (OAE 2, 94 Ma) signify two major carbon-cycle perturbations that lasted for 200 and 500 ky, respectively (Paul et al., 1994; Sageman et al., 2006). Both events were defined by a widely recorded marine $\delta^{13}C$ positive excursion, implying periods of unusually high productivity and excessive organic-carbon burial in the ocean (Paul et al., 1994; Jenkyns, 2010). In contrast to a >2‰ $\delta^{13}C$ excursion and prevalent ocean anoxia during OAE 2 (Jenkyns, 2010), MCE I was accompanied by a smaller (1‰) $\delta^{13}C$ excursion and only local deoxygenation (Paul et al., 1994; Coccioni and Galeotti, 2003). This event, however, shows many features in common with OAE 2, including migration of boreal fauna to mid-latitude seas and transient climate cooling (Paul et al., 1994; Gale and Christensen, 1996, Voigt et al., 2004; Barclay et al., 2010). MCE I has, consequently, been considered as a precursor to OAE 2 (Coccioni and Galeotti, 2003; Friedrich et al., 2009).

High productivity conditions assumed to characterize both events required increased nutrient supply to the upper ocean. In the case of OAE 2, an accelerated hydrological cycle, intensified silicate weathering and intense large igneous province (LIP) volcanism may have served as direct or indirect nutrient sources (Blattler et al., 2011; Pogge von Strandmann et al., 2013; Du Vivier et al., 2014; van Helmond et al., 2014). Upwelling of nutrient-rich deep waters may also have played a role during both events (Voigt et al., 2004; Jenkyns, 2010). The detailed mechanism that sustained continuous nutrient supply to the upper ocean over the long periods of these events remains unknown. However, ocean circulation must have been involved as a driver, as it directly distributes nutrients in seawater (Jimenez Berrocoso et al., 2010; Du Vivier et al., 2014), although its exact role is unclear. Alternative states of ocean

74 circulation (e.g. largely stagnant *vs* vigorous) have been proposed for the mid-
75 Cretaceous (e.g. Arthur et al., 1987; Martin et al., 2012).

76 This study uses Nd isotopes (expressed by $\varepsilon Nd(t)$) to track changes of ocean
77 circulation in the European epicontinental Chalk Sea during MCE I. Watermasses in
78 the ocean are tagged by characteristic $\varepsilon Nd(t)$ from surrounding continents, and their εNd
79 signatures are maintained during circulation (e.g. Jeandel et al., 2007). Distinct
80 seawater $\varepsilon Nd(t)$ values in major ocean basins during the mid-Cretaceous allow for tracing
81 of watermasses with different origins (Pacific: −2 to −4; Tethys: −4 to −8; Atlantic: −
82 6 to −8; European epicontinental sea: −8 to −10) (e.g. Puceat et al., 2005; Robinson et al.,
83 2010; Murphy and Thomas, 2012).

84 Nd isotopes revealed a change in the source of water in the European
85 epicontinental Chalk Sea in response to transient climate cooling during OAE 2
86 (Zheng et al., 2013). This study examines whether such a circulation-climate
87 coupling is unique to OAE 2 by tracing seawater $\varepsilon Nd(t)$ in the same area during the
88 analogous MCE I. In addition, prominent $\varepsilon Nd(t)$ positive excursions were observed in the
89 European epicontinental sea and Demerara Rise in the tropical Atlantic during OAE
90 2, and were explained by either a change of circulation or advection of radiogenic Nd
91 from intense volcanism during the event (MacLeod et al., 2008; Martin et al., 2012,
92 Zheng et al., 2013). These possibilities may be resolved by tracing seawater $\varepsilon Nd(t)$ across
93 MCE I, for which there is no accompanying evidence of major volcanic pulses.

94

95 **SECTION BACKGROUND**

96 We sampled an ~11 m-thick section of the English Chalk exposed at Lydden
97 Spout in Folkestone (UK, 51.10°N, 1.26°E). The section comprises a sequence of
98 foraminiferal-nannofossil chalk-marl couplets, which have been numbered and

99 considered to represent ~20 kyr-precession cycles (Paul et al., 1994; Gale, 1995). A
100 double-peak $\delta^{13}C$ positive excursion defining MCE I was reported from an outcrop at
101 Abbot's Cliff (Paul et al., 1994), ~200 m away to the west of the outcrop studied here.
102 The section is interpreted as having deposited in shallow waters (<1000 m) in a
103 pelagic epicontinental environment at the jw1ction of the Boreal Sea, Tethys and
104 proto-North Atlantic during the mid-Cretaceous (Fig. 1).

105 Two widely traceable beds in the section, the lower one at the basal couplet
106 B41 (*arlesiensis* Bed) and the upper one at the basal couplet C1 (*primus* Bed), contain
107 abundant faunas of boreal affinity (Fig. 2) (Paul et al., 1994; Gale 1995), notably two
108 species of bivalve, *Chlamys arlesiensis* (Woods) and *Oxytoma seminudum* (Dames),
109 and a nektonic belemnite, *Actinocamax primus* (Arkhangelsky). These boreal species
110 also occur widely in European basins at levels equivalent to Bed 4-8 of the upper
111 Cenomanian Plenus Marls during OAE 2 (Fig. 2), where *A. primus* is replaced by the
112 descendant species *A. plenus* (Blainville) (Gale and Christensen, 1996).

113

114 **MATERIALS AND METHODS**

115 $\delta^{13}C$ was measured on bulk chalk every ~5 cm. Seawater εNd was measured on
116 fish debris collected from 23 stratigraphic levels at ~50-cm spacing, and
117 supplemented by measurements on acetic acid extracted carbonates from bulk chalk
118 from 10 additional levels. Paired fish debris and carbonates from 8 stratigraphic levels
119 were measured to compare εNd values of the two archives. To assess tl1e possible use
120 of carbonates in chalk sections for seawater εNd reconstruction in future studies, εNd
121 was also measured on carbonates from 10 stratigraphic levels in a European reference
122 chalk section for OAE 2 at Eastbourne, and then compared with the published fish-
123 debris εNd values from identical levels (Zheng et al., 2013). εNd values were corrected

124 for radiogenic ingrowth. Details on extraction of fish debris and carbonates, and
125 analytical protocols are availble in the GSA Data Repository.
126
127 **RESULTS**
128 $\delta^{13}C$ rises from -1.9‰ near the base of couplet B38 towards peak values of
129 -2.5‰ in the *arlesiensis* Bed at couplet B41 (Fig. 2). After a trough of -2.2‰ at
130 couplet B42-B43, $\delta^{13}C$ rises to -2.5‰ again towards the top of the *primus* Bed at
131 couplet C1 before decreasing from the upper couplet C2. Stratigraphic positions of
132 this double-peak $\delta^{13}C$ positive excursion defining MCE I agrees with that reported
133 from the nearby Abbot's Cliff (Paul et al., 1994).
134 Fish debris and carbonates from the same stratigraphic Levels recorded
135 identical εNd values (Fig. 2), validating construction of a composite εNd record using
136 data from both archives. εNct starts to decrease from background values of ~-9 at the
137 uppermost couplet B39, one couplet above the onset of the $\delta^{13}C$ rise at lower couplet
138 B38. It continues to decrease towards a minima of ~-10 in the *arlesiensis* Bed during
139 the first $\delta^{13}C$ rise. Above that, εNd returns to background values while $\delta^{13}C$ decreases
140 from its first peak. Up-section, εNd decreases again from the upper couplet B42, and
141 reaches a minima of ~-10 within the *primus* Bed, being followed by an abrupt εNd
142 reversal to background values, and then by another -1-unit decrease roughly at the
143 level of the second *b* $\delta^{13}C$ peak. εNct finally recovers to background values at the end of
144 the $\delta^{13}C$ excursion.
145 The stratigraphy of the εNd negative excursions corresponds closely with the
146 levels containing boreal faunas, but the onset of the first and second εNd drop predates
147 the first appearance of these fossils at the *arlesiensis* Bed and the *primus* Bed
148 respectively, although the second εNd excursion is intenupted by a rapid εNd reversal

149 within the *primus* Bed, and followed by a third ε_{Nd} negative excursion over the
150 interval containing boreal faunas.
151
152 DISCUSSION
153 Origin of the ε_{Nd} record across the MCE I interval
154 The composite ε_{Nd} record across MCE I represents bottom-water signatures,
155 rather than late diagenetic overprints. Fish debris incorporates seawater Nd on the
156 seafloor, thereby recording bottom-water ε_{Nd} values (Martin and Scher, 2004). High
157 Nd concentration of fish debris (commonly >500 ppm, Table DR2) and low clay
158 content (<20 wt%, Paul et al., 1994) throughout the studied section should minimize
159 overprint of fish-debris ε_{Nd} by detrital values in the sediments, an assertion supported
160 by the lack of co-variation between ε_{Nd} and lithology (Fig. 2).
161 The chalks themselves appear to record bottom-water ε_{Nd}, because they have
162 values identical to those preserved in fish debris from the same stratigraphic levels
163 (Fig. 2). The good agreement between the two archives in two sections, covering
164 different mid-Cretaceous periods, highlights the potential use of bulk carbonates as a
165 simple substitute for future high-resolution seawater ε_{Nd} reconstructions in Cretaceous
166 chalk sections.
167
168 Nd-isotope inferred reorganizations of ocean circulation during MCE I
169 Both tropical and Norwegian seaways were open during the mid-Cretaceous
170 (Fig. 1), so seawater ε_{Nd} in the European epicontinental sea may have been affected
171 by upper circulation connecting the Tethys and North Atlantic, and by boreal
172 seawater. A broadly westward-flowing circum-global current has been proposed as a
173 dominant feature of upper ocean circulation at low and mid-latitudes during the

174 Cretaceous (Fig. 1), and relatively high ε_{Nd} values (~ -4 to -9) found in shallow and
175 intermediate waters at mid-latitudinal North Atlantic sites and east Tethys during the
176 Cretaceous have been explained by advection of Pacific seawater with high ε_{Nd} values
177 via the circum-global current (Puceat et al., 2005; Martin et al., 2012). Circulation
178 flowing between the Atlantic and Tethys may, therefore, have had a radiogenic ε_{Nd}
179 signature. In contrast, boreal seawater likely had low ε_{Nd} values, because of
180 weathering input from surrounding Precambrian continents characterized by ε_{Nd}
181 between ~ -17 and -30 (Jeandel et al., 2007). A seawater ε_{Nd} value of ~ -17 has been
182 found from the boreal realm for the upper Cretaceous (Puceat et al., 2005).

183 Relatively invariant background ε_{Nd} values (~ -9) indicate stable ocean
184 circulation in the European epicontinental sea before and after MCE I. This
185 circulation pattern was not uncommon during the mid-Cretaceous, as similar seawater
186 ε_{Nd} values persisted in this area before OAE 2 (Zheng et al., 2013) (Fig. 2). Recurrent
187 ε_{Nd} negative excursions during MCE I (Fig. 2) are interpreted to reflect transient
188 increases in the influence of boreal seawater in the European epicontinental sea. This
189 interpretation is consistent with the close association between the inferred
190 strengthening of boreal seawater and migration of boreal faunas. Although enhanced
191 weathering of surrounding Precambrian continents may lower seawater ε_{Nd} values, the
192 recurrent, rapid and reversible nature of the ε_{Nd} negative excursions is difficult to
193 reconcile with changes in continental weathering. Furthermore, pulses of intensified
194 weathering are not supported by temperature reconstructions that show little climatic
195 warming during MCE I (Voigt et al., 2004; Moriya et al., 2007; Ando et al., 2009).

196 Modelling results suggest that ocean circulation in the European
197 epicontinental sea was sensitive to tectonics or sea-level changes during the mid-
198 Cretaceous (Poulsen et al., 1998). However, slow and irreversible tectonic movements

199 cannot explain the transient and recunent circulation reorganizations. A sea-level
200 control may also be precluded, because the inferred circulation changes are not in-
201 phase with reconstructed sea-level changes during MCE I (Fig. 2).
202
203 A **climatic control on circulation reorganizations during MCE I and OAE 2**
204 The onset of the period with episodic increases of boreal influence in bottom
205 waters in the European epicontinental sea, marked by the first ε_{Nd} negative excursion,
206 lagged the onset of $\delta^{13}C$ rise of MCE I. This lead-lag relationship is identical to that
207 observed for OAE 2 in the same area (Fig. 2), where enhanced influence of boreal
208 seawater, suggested by a similar 1-unit ε_{Nd} negative excursion, occurred after the
209 onset of the $\delta^{13}C$ rise of OAE 2 (Zheng et al., 2013). These records reveal a consistent
2 10 response of ocean circulation to changes in the carbon cycle during both events.
211 Enhanced organic carbon burial during OAE 2 is expected to have sequestered
212 atmospheric C02, leading to intermittent climate cooling during the event (Forster et
213 al., 2007; Barclay et al., 2010; Jarvis et al., 2011; van Helmond et al., 2014). The
214 onset of circulation change during OAE 2 coincided with such a cooling (Fig. 2)
215 (Zheng et al., 2013). This coincidence is explained by a prompt circulation response
216 to climate-induced fluctuations in the latitudinal thermal gradient that may have
217 destabilized the ocean (Forster et al., 2007; Zheng et al., 2013).
218 The same climate forcing may explain circulation reorganizations during MCE
219 I, because enhanced organic-carbon burial during this event can in principle have
220 caused episodic atmospheric C02 drawdown, albeit at a smaller magnitude compared
221 to OAE 2. The broad correlation between ε_{Nd} drops and $\delta^{13}C$ peaks during MCE I,
222 similarly observed during OAE 2, is compatible with a link between circulation
223 changes and marine carbon burial (Fig. 2). Transient 2°C cooling during MCE I is

224 suggested by $\delta^{18}O$ records from the mid-latitudinal and subtropical European shelf sea
225 and North Atlantic (Voigt et al., 2004).
226
227 Implications for the cause of the ε_{Nd} positive excursion during OAE 2
228 An obvious difference in ε_{Nd} records from the European epicontinental sea for
229 MCE I and OAE 2 is the presence of an ε_{Nd} positive excursion during OAE 2 (Fig. 2).
230 Prominent ε_{Nd} increases, found in the European epicontinental sea and Demerara Rise
231 in the tropical Atlantic during OAE 2, have been considered to reflect either climate-
232 induced intensification of high ε_{Nd} waters from the Tethys or North Atlantic (Martin
233 et al., 2012), or advection of radiogenic Nd released from LIP volcanisms under
234 anoxic conditions (Zheng et al., 2013). Considering analogous carbon-cycle variations
235 and the similar response of European epicontinental circulation during both events, if
236 an ε_{Nd} positive excursion during OAE 2 resulted purely from a circulation change, it
237 would be predicted for MCE I. However, no ε_{Nd} increase is seen across the MCE I
238 record, reflecting either the absence of major LIP volcanisms such as those
239 punctuated OAE 2 (Du Vivier et al., 2014), or the absence of sufficient anoxia
240 required to mobilize volcanic Nd. Both possibilities are, however, support a volcanic
241 origin for the ε_{Nd} positive excursion during OAE 2 (Zheng et al., 2013).
242
243 A climatic control on boreal faunal migration during MCE I and OAE 2
244 The three boreal fauna! events, two during MCE I and one during OAE 2 (i.e.
245 Plenus Cold Event; Paul et al., 1994; Gale and Christensen, 1996), can be explained
246 either by passive transport of fauna by relatively cold boreal waters, or by a biological
247 response to climate-induced cooling of the ocean. The ε_{Nd} records of MCE I and OAE
248 2 favor the latter explanation as the primary cause for these migrations, because the

fast appearance of boreal faunas in the European epicontinental sea for the three faunal intervals invariably took place after the influence of boreal seawater was increased (Fig. 2). Ocean circulation responded more quickly to climate forcing, as biology may not respond until a particular climatic threshold was crossed.

Implications for the maintenance of MCE I and OAE 2

This study shows a prompt response of ocean circulation to changes in the carbon cycle during MCE I and OAE 2. Such a high circulation-climate sensitivity is not revealed by previous modelling results (Poulsen et al., 2001). Transient reorganizations of ocean circulation, probably in response to brief atmospheric C02 drawdown during both events, may have helped replenish surface waters with nutrients from deep waters and/or LIP sources, providing a critical positive feedback that sustained high-productivity conditions of MCE I and OAE 2 over hundreds of thousands of years.

ACKNOWLEDGMENTS

Supported by the University of Oxford Clarendon Scholarship to X.-Y. Zheng. We thank Stuart Robinson and Martin Frank for helpful comments.

REFERENCES CITED

Ando, A, Huber, E.T., MacLeod, K.G., Ohta, T., and Khim, B.-K., 2009, Blake Nose stable isotopic evidence against the mid-Cenomanian glaciation hypothesis: Geology, v. 37, p. 451-454, doi: 10.1130/G25580A.1.

Arthur, M.A., Schlanger, S.O., and Jenkyns, H.C., 1987, The Cenomanian-Turonian Oceanic Anoxic Event, II. Palaeoceanographic controls on organic-matter production and preservation: Geological Society, London, Special Publications, v. 26, p. 401-420, doi:10.1144/GSL.SP.1987.026.01.25.

Barclay, RS., McElwain, J.C., and Sageman, B.B., 2010, Carbon sequestration activated by a volcanic C02 pulse during Ocean Anoxic Event 2: Nature Geoscience, v. 3, p. 205-208, doi:10.1038/ngeo757.

279 Blattler, C.L., Jenkyns, H.C., Reynard, L.M. and Henderson, G.M., 2011, Significant
280 increases in global weathering during Oceanic Anoxic Events 1a and 2
281 indicated by calcium isotopes, Earth and Planetary Science Letters, v. 309, p.
282 77-88, doi:10.1016/j.epsl.2011.06.029.
283 Coccioni, R., and Galeotti, S., 2003, The mid-Cenomanian Event: prelude to OAE 2:
284 Palaeogeography, Palaeoclimatology, Palaeoecology, v. 190, p. 427-440,
285 doi: 10.1016/S0031-0182(02)00617-X.
286 Du Vivier, A.D.C., Selby, D., Sageman, B.B., Jarvis, I., Grocke, D.R., and Voigt, S.,
287 2014, Marine $^{187}Os/^{188}Os$ isotope stratigraphy reveals the interaction of
288 volcanism and ocean circulation during Oceanic Anoxic Event 2: Earth and
289 Planetary Science Letters, v. 389, p. 23-33, doi:10.1016/j.epsl.2013.12.024.
290 Forster, A., Schouten, S., Moriya, K., Wilson, P.A., and Sinninghe Damste, J.S.,
291 2007, Tropical warming and intermittent cooling during the
292 Cenomanian/Turonian oceanic anoxic event 2: sea surface temperature records
293 from the equatorial Atlantic: Paleoceanography, v. 22, PA1219,
294 doi:10.1029/2006PA001349.
295 Friedrich, O., Erbacher, J., Wilson, P.A., Moriya, K., and Mutterlose, J., 2009,
296 Paleoenvironmental changes across the Mid Cenomanian Event in the tropical
297 Atlantic Ocean (Demerara Rise, ODP Leg 207) inferred from benthic
298 foraminiferal assemblages: Marine Micropaleontology, v. 71, p. 28-40,
299 doi: 10.1016/j.marmicro.2009.01.002.
300 Gale, A.S., 1995, Cyclostratigraphy and correlation of the Cenomanian stage of
301 Europe: Special Publications of the Geological Society, v. 85, p. 177-197, doi:
302 10.1144/GSL.SP.1995.085.01.11.
303 Gale, A.S., and Christensen, W., 1996, Occurrence of the belemnite *Actinocamax*
304 *plenus* in the Cenomanian of SE France and its significance: Bulletin of the
305 Geological Society of Denmark, v. 43, p. 68-77.
306 Jarvis, I., Lignum, J.S., Grocke, D.R., Jenkyns, H.C. and Pearce, M.A., 2011, Black
307 shale deposition, atmospheric CO_2 drawdown, and cooling during the
308 Cenomanian-Turonian Oceanic Anoxic Event: Paleoceanography, v 26,
309 PA3201, doi: 10.1029/2010PA002081.
310 Jeandel, C., Arsouze, T., Lacan, F., Techine, P., and Dutay, J.-C., 2007, Isotopic Nd
311 compositions and concentrations of the lithogenic inputs into the ocean: a
312 compilation, with an emphasis on the margins: Chemical Geology, v. 239, p.
313 156-164, doi: 10.1016/j.chemgeo.2006.11.013.
314 Jenkyns, H.C., 2010, Geochemistry of oceanic anoxic events: Geochemistry
315 Geophysics Geosystems, v. 11, Q03004, doi:10.1029/2009GC002788.
316 Jimenez Berrocoso, A., MacLeod, K.G., Martin, E.E., Bourbon, E., Londono, C.I.,
317 and Basak, C., 2010, Nutrient trap for Late Cretaceous organic-rich black
318 shales in the tropical North Atlantic: Geology, v. 38, p. 1111-1114,
319 doi:10.1130/G31195.1.
320 MacLeod, K.G., Martin, E.E., and Blair, S.W., 2008, Nd isotopic excursion across
321 Cretaceous ocean anoxic event 2 (Cenomanian-Turonian) in the tropical North
322 Atlantic: Geology, v. 36, p. 811-814, doi: 10.1130/G24999A.1.
323 Martin, E.E., MacLeod, K.G., Jimenez Berrocoso, A., and Bourbon, E., 2012, Water
324 mass circulation on Demerara Rise during the Late Cretaceous based on Nd
325 isotopes: Earth and Planetary Science Letters, v. 327-328, p. 111-120,
326 doi:10.1016/j.epsl.2012.01.037.

Martin, E.E., and Scher, H.D., 2004, Preservation of seawater Sr and Nd isotopes in fossil fish teeth: bad news and good news: Earth and Planetary Science Letters, v. 220, p. 25-39, doi:l0.1016/S0012-821X(04)00030-5.

Moriya, K., Wilson, P.A., Friedrich, 0., Erbacher, J., and Kawabata, H., 2007, Testing for ice sheets during the mid-Cretaceous greenhouse using glassy foraminiferal calcite from the mid-Cenomanian tropics on Demerara Rise: Geology, v. 35, p. 615-618, doi:l0.1130/G23589A.l.

Murphy, D.P., and Thomas, D.J., 2012, Cretaceous deep-water formation in the Indian sector of the Southern Ocean: Paleoceanography, v. 27, PA1211, doi:l 0.1029/2011PA002198.

Paul, C.R.C., Mitchell, S.F., Marshall, J.D., Leafy, P.N., Gale, A.S., Duane, A.M., and Ditchfield, P.W., 1994, Palaeoceanographic events in the Middle Cenomanian of Northwest Europe: Cretaceous Research, v. 15, p. 707-738, doi:l0.1006/cres.1994.1039.

Pogge von Strandmann, P.A.E., Jenkyns, H.C., and Woodfine, R.G., 2013, Lithium isotope evidence for enhanced weathering during Oceanic Anoxic Event 2: Nature Geoscience, v. 6, p. 668-672, doi:l0.1038/ngeo1875.

Poulsen, C.J., Barron, E.J., Arthur, M.A., and Peterson, W.H., 2001, Response of the Mid-Cretaceous global oceanic circulation to tectonic and C02 forcings: Paleoceanography, v. 16, p. 576-592, doi:l0.1029/2000PA000579.

Poulsen, C.J., Seidov, D., Barron, E.J., and Peterson, W.H., 1998, The impact of paleogeographic evolution on the surface oceanic circulation and the marine environment within the mid-Cretaceous Tethys: Paleoceanography, v. 13, p. 546-559, doi:l 0.1029/98PA01789.

Puceat, E., Lecuyer, C., and Reisberg, L., 2005, Neodymium isotope evolution of NW Tethyan upper ocean waters throughout the Cretaceous: Earth and Planetary Science Letters, v. 236, p. 705-720, doi:l0.1016/j.epsl.2005.03.015 .

Robinson, S.A., Murphy, D.P., Vance, D., and Thomas, D.J., 2010, Formation of "Southern Component Water" in the Late Cretaceous: evidence from Nd-isotopes: Geology, v. 38, p. 871-874, doi: 10.1130/G31165.1.

Sageman, B.B., Meyers, S.R., and Arthur, M.A., 2006, Orbital time scale and new C-isotope record for Cenomanian-Turonian boundary stratotype: Geology, v. 34, p. 125-128, doi: 10.1130/G22074.1.

van Belmond, N.A.G.M., Sluijs, A., Reichart, G.-J., Sinninghe Damste, J.S., Slomp, C.P., and Brinkhuis, H., 2014, A perturbed hydrological cycle during Oceanic Anoxic Event 2: Geology, v. 42, p. 123-126, doi: 10.1130/G34929.1.

Voigt, S., Gale, A.S., and FlOgel, S., 2004, Midlatitude shelf seas in the Cenomanian-Turonian greenhouse world: temperature evolution and North Atlantic circulation: Paleoceanography, v. 19, PA4020, doi:10.1029/2004PA00 1015.

Wilmsen, M., 2003, Sequence stratigraphy and palaeoceanography of the Cenomanian Stage in northern Germany: Cretaceous Research, v. 24, p. 525-568, doi: l0.1016/S0195-667 1(03)00069-7.

Zheng, X.-Y., Jenkyns, H.C., Gale, A.S., Ward, D.J., and Henderson, G.M., 2013, Changing ocean circulation and hydrothermal inputs during Ocean Anoxic Event 2 (Cenomanian-Turonian): evidence from Nd-isotopes in the European shelf sea: Earth and Planetary Science Letters, v. 375, p. 338-348, doi: 10.1016/j.eps l.2013.05.053.

Figure 1. Paleogeographic map of the mid-Cretaceous (modified from Jarvis et al. 2011), showing the location of Lydden Spout section (star) and sites mentioned in the text (circle) along with seawater εNd values during the Cretaceous (Puceat et al., 2005; Martin et al., 2012). Ce = Cenomanian; Co = Coniacian; Maa = Maastrichtian. Inset map shows present-day locations of Lydden Spout and Eastbourne sections. Arrows imply the general pattern of ocean circulation during the mid-Cretaceous (Puceat et al., 2005).

Figure 2. $\delta^{13}C$ and εNd results plotted against the stratigraphic column of the Lydden Spout section across the MCE I interval. (A) red circles = bulk-carbonate $\delta^{13}C$; thick red line = 10-point moving average that brings out key features of the $\delta^{13}C$ record; vertical red dashed line = pre-MCE $\delta^{13}C$ values; gray line = carbonate $\delta^{13}C$ from nearby Abbot's Cliff (Paul et al., 1994); red arrow = the initial $\delta^{13}C$ rise of MCE I; gray band = MCE I, defined by a double-peak $\delta^{13}C$ positive excursion. (B) thick orange line = the composite εNd curve, which comprises data from fish debris (orange circles), carbonates (open black circles), and mean values (half-filled orange circles) where paired εNd results (fish debris = pink squares; carbonates = blue diamonds) are available; green vertical bar = typical εNd mid-Cretaceous background values; orange arrow = the onset of the first εNd decrease. (C) black curve = sea-level reconstruction (Wilmsen, 2003). Graded yellow bands = levels of boreal faunas with darker yellow indicating the two faunal beds (the *arlesiensis* and *primus* Bed) where boreal faunas are abundant (Paul et al., 1994). (D) the εNd record (orange) from the chalk section at Eastbourne across the OAE 2 interval (grey band), together with the $\delta^{13}C$ curve (grey), is shown for comparison (Zheng et al., 2013). Green vertical bar = pre-OAE εNd values; red bar = an inferred volcanic pulse, coincident with the positive εNd

excursion; yellow band = levels of boreal faunas (the Plenus Marl Beds 4-8; i.e. Plenus Cold Event); blue bar = a transient cooling phase inferred from combined geochemical and faunal evidence from the Eastbourne section (Zheng et al., 2013). Dashed lines "a" and "b" in (A) (B) and (D) mark the onset of the $\delta^{13}C$ positive excursion and the beginning ofreorganization of circulation, respectively.

Figure_1

Click here to download Figure Xinyuan Zheng_Fig_1.eps

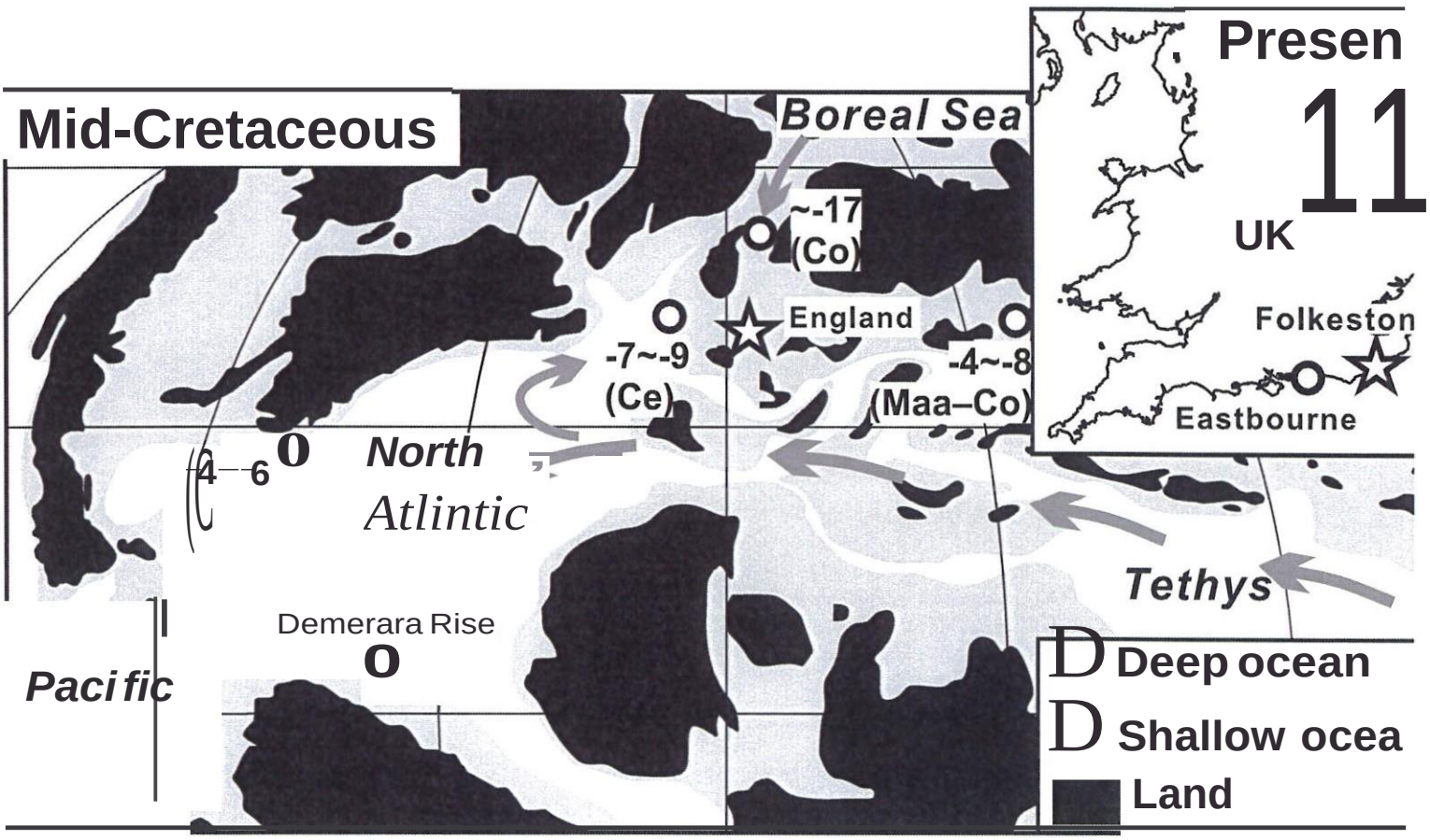

Figure_2

Click here to downbatj y2n Zheng_Fig_2.eps

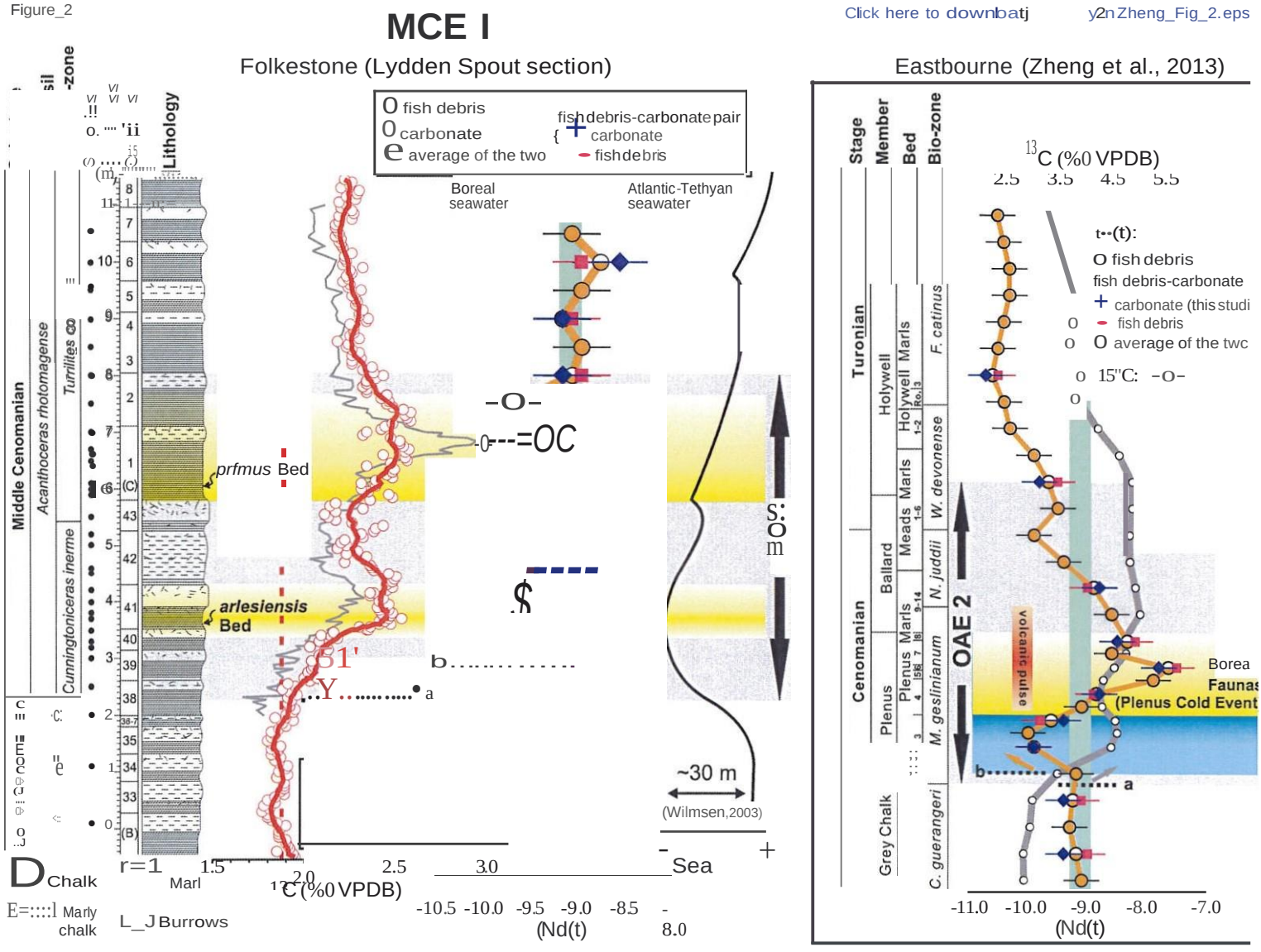

Supplementary materials

A climatic control on reorganization of ocean circulation during the mid-Cenomanian Event and Cenomanian-Turonian oceanic anoxic event (OAE-2): Nd-isotope evidence

Xin-Yuan Zheng, Hugh C. Jenkyns, Andrew S. Gale,
David J. Ward, and Gideon M. Henderson

1. Sample preparation

Fish debris was extracted from bulk chalks using a method described in Zheng et al. (2013). Carbonate fractions of bulk chalk were removed by dissolving in ~7.5% (v/v) formic acid, buffered to a pH of ~3.2 with ~7.5% (v/v) calcium acetate solution, for 1–3 days. Fish debris was then handpicked from the residues under a binocular microscope. Fish debris was cleaned by a reductive-oxidative protocol to remove Fe-Mn oxides and attached fine clays (Boyle, 1981; Boyle and Keigwin, 1985; Rosenthal et al., 1997), and then dissolved in 6 M quartz-distilled HCl at ~120°C for at least 12 h. Dissolved fish-debris samples were split into two aliquots for measurement of Nd isotopes and Sm/Nd ratios.

Carbonate fractions of bulk chalk from several stratigraphic levels were also measured for Nd isotopes to increase temporal resolution of the $\varepsilon_{Nd}(t)$ record across MCE I. Large chunks of chalk (> 10 g) were ground into powder using an agate pestle and mortar. About 5 g of powder was leached using 10% (v/v) distilled acetic acid at

room temperature for ~2 h before being centrifuged, and supernatant liquid was then taken for elemental and Nd isotopic analysis.

2. Analytical protocols

2.1. Bulk chalk $\delta^{13}C$

Bulk chalk $\delta^{13}C$ was measured using a VG Isogas Prism IImass spectrometer with an on-line VG Isocarb common acid bath preparation system. Carbonate powders were dosed with acetone and dried at 60°C for at least 30 minutes. In the instrument they were reacted with purified phosphoric acid at 90°C. Calibration to the VPDB standard via NBS-19 was made daily using the in-house (NOCZ) Carrara Marble standard. Reproducibility of $\delta^{13}C$ measurement is better than 0.1%0 (Io).

2.2. Nd isotopes, Nd/Sm ratios and in-growth correction

Nd isotopes were measured on an MC-ICP-MS (Nu plasma) after purification of Nd with a two-stage ion-exchange chromatographic separation. The first stage used AG 50W-X12 resin (Bio-Rad, 200-400 mesh, H form) and HCI as an eluent to separate REEs from major matrix ions, and the second stage adopted AG 50W-X4 (Bio-Rad, 200-400 mesh, ammonium fonn) and a-hydroxyisobutyric acid (a-HIBA) as an eluent to separate Nd from other REEs. The procedural blank of <50 pg Nd was negligible compared to >120 ng Nd processed through column separation. Instrumental mass bias was corrected by using $^{146}Nd/^{144}Nd = 0.7219$ and the exponential fractionation law. Repeated measurement of JNdi-1 yielded $^{143}Nd/^{144}Nd = 0.512099 \pm 0.000017$ (n=301, 2o), which is in good agreement with the published consensus value (Tanaka et al., 2000). Repeated analysis of a fish bone composite standard yielded $^{143}Nd/^{144}Nd = 0.512364 \pm 0.000013$ (n=21, 2o), which also agrees

with inter-laboratory calibration results (Scher and Delaney, 20 ɹ 0). Long-term reproducibility of Nd-isotope analysis is estimated to be 0.3 εNd unit (2cr).

All εNd values reported in this shidy were corrected for radiogenic in-growth of ^{143}Nd from ^{147}Sm. Sm/Nd ratios that were measured on an HR-ICP-MS (Element 2) using indium as an internal standard. Repeated measurement on a gravimetrically prepared REE solution indicated that the measured Sm/Nd ratios agreed with its gravimetric value within l%. Long-term reproducibility of the Sm/Nd ratio, based on measurements of the gravimetrically prepared REE solution and a fish bone composite standard, is estimated to be better than **1%** (lcr).

For ^{143}Nd in-growth cotTection, the age model was based on cyclostratigraphy that considers each chalk-marl couplet to be controlled by a 20 kyr-precession cycle (Gale et al., 1999), and the base of the C. *inerme* Zone was tied to 96.50 Ma according to the Geological Time Scale (GTS) 2012 (Gradstein et al., 2012).

References

Boyle E. A. (1981) Cadmium, zinc, copper, and barium in foraminifera tests. *Earth Planet. Sci. Lett.* **53,** 11-3S.

Boyle E. A. and Keigwin L. D. (198S) Comparison of Atlantic and Pacific paleochemical records for the last 2 lS,000 years: changes in deep ocean circulation and chemical inventories. *Earth Planet. Sci. Lett.* **76,** 13S-1SO.

Gale A. S., Young J. R., Shackleton N. **J.,** Crowhurst S. J. and Wray D. S. (1999) Orbital tuning of Cenomanian marly chalk successions: towards a Milankovitch time-scale for the Late Cretaceous. *Philosophical Transactions of the Royal Society of London. Series A: Mathematical, Physical and Engineering Sciences* **357,** 181S-1829.

Gradstein F. M., Ogg }. G., Schmitz M. and Ogg G. (2012) The Geologic Time Scale 2012. 2-Volume Set (1st edition). Elsevier.

Rosenthal Y., Boyle E. A. and Labeyrie L. (1997) Last Glacial Maximum Paleochemistry and Deepwater Circulation in the Southern Ocean: Evidence From Foraminiferal Cadmium. *Paleoceanography* **12,** 787-796.

Scher H. D. and Delaney M. L. (2010) Breaking the glass ceiling for high resolution Nd isotope records in early Cenozoic paleoceanography. *Chem. Geol.* **269,** 329-338.

Tanaka T., Togashi S., Kamioka H., Amakawa H., Kagami H., Hamamoto T., Yuhara M., Orihashi Y., Yoneda S., Shimizu H., Kunimaru T., Takahashi K., Yanagi

T., Nakano T., Fujimaki H., Shinjo R., Asahara Y., Tanimizu M. and Dragusanu C. (2000) JNdi-1: a neodymium isotopic reference in consistency with LaJolla neodymium. *Chem. Geol.* **168,** 279-281.

Zheng X.-Y., Jenkyns H. C., Gale A. S., Ward D. J. and Henderson G. M. (2013) Changing ocean circulation and hydrothermal inputs during Ocean Anoxic Event 2 (Cenomanian-Turonian): evidence from Nd-isotopes in the European shelf sea. *Earth Planet. Sci. Lett.* **375,** 338-348.

Table DR1

Results of bulk-carbonate $15^{13}C$

J lcight (m)	$\delta^{13}C$ (‰$_{VPDB}$)	Height (m)	5''C (%.,.,,,,)	Height (m)	a''C (%.,,,)
-0.50	1.95	2.35	I96	4 80	2.34
-0.45	1.94	2.40	1.92	4.85	2.23
-0.40	I 85	2 45	I SS	4 90	2.29
-0.35	1.92	2.50	1.95	4.95	2.18
-0.30	1.91	2.55	1.91	5.00	2.23
-0.25	1.90	2.60	2. 10	*5.05*	2.20
-0.20	1.90	2.60	2.03	5. 10	2.22
-0.15	1.86	2.65	2.00	5. 15	2.32
-0. 10	1.86	2.65	2.07	5.20	2.31
-0.05	1.86	2.70	2. 11	5.25	23S
0.00	1.87	2.75	2 02	5.30	2.39
005	I90	2.80	2 04	5.35	2.43
0.10	1.85	2.85	2.05	5.40	2.26
0.15	1.82	2.90	2. 10	5.45	2.17
O W	1.80	2.95	2 04	*5.50*	2.13
0 25	1.80	3.00	2 10	*5.55*	2.11
0.30	1.77	3.05	2.08	5.60	2.17
0.35	I.SI	3.10	2.12	5.65	2.32
0.40	1.78	3.15	2.13	5.70	2.14
0.45	1.84	3.20	2 03	5.75	2.17
0.50	1.80	3.25	2.11	5.80	2.36
0.55	I84	330	2 08	*5* 85	2.48
060	1.89	3.35	2.18	5.90	2.46
0.65	1.87	3.40	2.09	*5.95*	2.35
0.70	1.89	3.45	2. 16	6.00	2.31
0.75	1.89	3.50	2 34	6.05	2.39
0.80	1.89	3.50	2.35	6.10	2.31
0.85	1.87	3.55	2.36	6.15	2.39
0.90	1.85	3.55	2.30	6.20	2.48
0.95	1.91	3.60	247	6.25	2.45
1.00	1.86	3.60	2.41	6.30	2.48
1.05	1.90	365	2.41	6.35	2.49
1.10	1.91	3.65	2.44	6.40	2.34
1.15	1.86	3.70	2 46	6.45	2.47
1.20	1.84	3.70	2 53	6.50	2.56
1.25	1.87	3.75	2.47	*6.55*	2.55
I.JO	1.82	3.75	2.43	6.60	2.43
1.35	1.85	3.80	2.42	6.65	2.55
1.40	1.82	3.80	2.48	6.70	2.57
1.40	1.82	3.85	2.41	6.75	2.54
1.45	1.84	3.85	2.46	680	2.52
1.45	1.87	3.90	2.40	6.85	**2.52**
1.50	1.82	3.95	2.46	6.90	2.47
1.55	1.80	4.00	2.41	6.95	2.32
1.60	1.82	4.05	2.43	7.00	2.34
1.65	1.84	4.10	2.36	7.05	2.42
1.70	1.82	4.15	2.38	7. 10	2.44
1.75	1.86	4. 15	2.36	7. 15	2.48
1.80	1.90	4.20	2.45	7.20	2.5S
1.85	I88	4.25	2 48	7.25	2.56
1.90	1.94	4.30	2.45	7.30	2.55
1.95	1.84	4.35	2 4S	7 35	2.58
i.95	1.90	4.40	2.49	7 40	2.54
2.00	1.90	4.45	2 *50*	7.45	2.48
2.05	1.94	4.50	2.46	7.50	2.45
2. 10	1.95	4.55	2 38	7.55	2.46
2. 15	1.92	4.60	2 37	7.60	**2.42**
2.20	1.91	4.65	2.36	7.65	2.45
2.25	1.93	4.70	2.22	7.70	2.34
2.30	1.91	4.75	2.33	7.75	2.34

Table DR1 (continued)

Results of bulk-carbonate $\delta^{13}C$

Height (m)	ll"C (%ovrou)	Height (m)	ll"C (%•vruu)	Height **(m)**	o"C (%•wuu)
7.80	2.32	9.05	2.30	10.35	2.19
7.85	2.34	9.10	2.30	10.40	2.20
7.90	234	9.15	2.32	10.45	2.17
7.95	2.39	9.20	2.29	10.50	2.19
8.00	2.43	9.25	2.28	10.55	2.18
8.05	2.38	9.30	2.29	10.60	2.17
8.10	2.32	9.35	2.28	10.65	2.17
8.15	2.37	9.40	2.26	10.70	2.19
8.20	2.26	9.45	2.28	10.75	2.26
8.25	2.26	9.50	2.31	10.80	2.19
8.30	2.31	9.55	2.24	10.85	2.27
8.35	2.26	9.60	2.25	10.90	2.26
8.40	2.30	9.65	2.21	10.95	2.20
8.45	2.26	9.70	2.24	11.00	2.23
8.50	2.23	9.75	2.23	11.05	2.19
8.55	2.24	9.80	2.26	11.10	2.28
8.60	2.18	9.85	2.25	11.15	2.23
8.65	2.30	9.90	2.32	I 1.20	2.29
8.70	2.25	9.95	2.2 I	I 1.25	2.30
8.75	2.27	10.00	2.23	I 1.30	2.20
8.80	2.27	10.05	2.22	I 1.35	2.25
8.85	2.27	10.10	2.22	I 1.40	2.26
8.90	2.25	10.15	2.26	11.45	2.22
8.95	2.34	10.25	2.21		
9.00	2.35	10.30	2.20		

Table DR2
Results of ε_{Nd} for MCE I

Sample	Height (m)	Age' (Ma)	$^{143}Nd/^{144}Nd(0)$	2a	$^{147}Sm/^{144}Nd$			[Nd] (ppm)
FISH DEBRIS								
LS05a	-0.5	96.592	0.512148	0.000005	0.1218	-9.6	-8.6	701
LS04a	0.0	96.575	0.512118	0.000010	0.1268	-10.1	-9.3	1724
LS03a	0.5	96.559	0.512136	0.000009	0.1229	-9.8	-8.9	766
LS02a	1.0	96.542	0.512126	0.000006	0.1221	-10.0	-9.1	6875
LS01a	1.5	96.525	0.512106	0.000009	0.1211	-10.4	-9.4	2930
LS1	2.0	96.508	0.512116	0.000009	0.1208	-10.2	-9.3	857
LS2	2.5	96.492	0.512124	0.000010	0.1224	-10.0	-9.1	203
LS3	3.0	96.475	0.512128	0.000008	0.1205	-9.9	-9.0	572
LS4	3.5	96.458	0.512077	0.000007	0.1266	-10.9	-10.1	3757
LS5	4.0	96.441	0.512107	0.000010	0.1154	-10.4	-9.4	1133
LS6	4.5	96.425	0.512122	0.000008	0.1231	-10.1	-9.2	888
LS7	5.0	96.408	0.512124	0.000010	0.1204	-10.0	-9.1	382
LS8	5.5	96.391	0.512102	0.000009	0.1190	-10.4	-9.5	738
LS9	6.0	96.374	0.512092	0.000008	0.1259	-10.7	-9.8	60
LS10	6.5	96.358	0.512113	0.000011	0.1196	-10.2	-9.3	291
LS1a	7.0	96.341	0.512089	0.000007	0.1215	-10.7	-9.8	641
LS2a	7.5	96.324	0.512097	0.000006	0.1238	-10.6	-9.7	95
LS3a	8.0	96.307	0.512128	0.000008	0.1209	-9.9	-9.0	757
LS4a	8.5	96.291	0.512129	0.000011	0.1205	-9.9	-9.0	251
LS5a	9.0	96.274	0.512123	0.000007	0.1223	-10.1	-9.1	191
LS6a	9.5	96.257	0.512127	0.000008	0.1207	-10.0	-9.0	
LS7a	10.0	96.240	0.512127	0.000007	0.1196	-10.0	-9.0	98
LS8a	10.5	96.224	0.512127	0.000007	0.1217	-10.0	-9.1	855
BULK CARBONATE								
LS02a_carb	1.0	96.542	0.512119	0.000006	0.1146	-10.1	-9.1	
LS2_carb	2.5	96.492	0.512125	0.000010	0.1034	-10.0	-8.9	
LSP6_carb	3.2	96.468	0.512100	0.000008	0.1127	-10.5	-9.5	
LSP7_carb	3.3	96.465	0.512089	0.000007	0.1091	-10.7	-9.6	
LS4_carb	3.5	96.458	0.512073	0.000009	0.1104	-11.0	-10.0	
LSP11_carb	3.7	96.451	0.512072	0.000008	0.1132	-11.0	-10.0	
LSP12_carb	3.8	96.448	0.512091	0.000008	0.1207	-10.7	-9.7	
LSP16_carb	4.2	96.435	0.512106	0.000008	0.1144	-10.4	-9.4	
LSP20_carb	4.6	96.421	0.512112	0.000008	0.1115	-10.3	-9.2	
LS7_carb	5.0	96.408	0.512121	0.000008	0.1092	-10.1	-9.0	
LSP25_carb	5.2	96.401	0.512107	0.000008	0.1177	-10.3	-9.4	
LSP31_carb	5.9	96.378	0.512084	0.000008	0.1084	-10.8	-9.7	
LS9_carb	6.0	96.374	0.512107	0.000009	0.1126	-10.3	-9.3	
LSP33_carb	6.1	96.371	0.512119	0.000008	0.1161	-10.1	-9.1	
LSP39_carb	6.7	96.351	0.512109	0.000008	0.1050	-10.3	-9.2	
LS3a_carb	8.0	96.307	0.512113	0.000007	0.1151	-10.2	-9.2	
LS5a_carb	9.0	96.274	0.512108	0.000008	0.1061	-10.3	-9.2	
LS7a_carb	10.0	96.240	0.512141	0.000008	0.1083	-9.7	-8.6	

'Age model was based on Gradstein et al. (2012);

$\varepsilon_{Nd}(t) = \{[^{143}Nd/^{144}Nd_{measured}(t)/^{143}Nd/^{144}Nd_{CHUR}(t)] - 1\} \times 10^4$; $^{143}Nd/^{144}Nd(t) = ^{143}Nd/^{144}Nd(0) - ^{147}Sm/^{144}Nd(0) \times (EXP(\lambda_{Sm} \times T) - 1]$;

λ_{Sm} (decay constant of ^{147}Sm) = 6.54×10^{-12} y^{-1}; T: age; $^{143}Sm/^{144}Nd_{CHUR}(0) = 0.1967$, $^{143}Nd/^{144}Nd_{CHUR}(0) = 0.512638$.

Table DR3

Results of εNd in acetic acid extracted carbonates for OAE 2

Sample	Height	Age•	Bulk Carbonate					Fish Debris•	
	(m)	(Ma)	$^{143}Nd/^{144}Nd$	2SE	$^{147}Sm/^{144}Nd$	ENd(O)	ENd(t)	ENd(O)	ENd(t)
HC2	1	94.08	0.512103	0.000009	0.1166	-10.4	-9.5	-10.0	-9.1
HC4	3	94.00	0.512092	0.000007	0.1043	-10.7	-9.5	-10.2	-9.2
HC6	5	93.91	0.512080	0.000006	0.1206	-10.9	-10.0	-10.9	-10.0
HC7	6	93.86	0.512104	0.000006	0.1177	-10.4	-9.5	-10.8	-9.9
HC8	7	93.82	0.512129	0.000007	0.1100	-9.9	-8.9	-9.9	-9.0
HC9	8	93.78	0.512187	0.000007	0.1179	-8.8	-7.9	-8.4	-7.5
HC10	9	93.73	0.512157	0.000007	0.1278	-9.4	-8.6	-9.1	-8.3
HC12	11	93.65	0.512127	0.000007	0.1088	-10.0	-8.9	-10.2	-9.2
HC16	15	93.49	0.512072	0.000007	0.0982	-11.0	-9.9	-10.7	-9.7
HC20	19	93.34	0.512030	0.000007	0.1055	-11.9	-10.8	-11.7	-10.7

'Age model was based on Voigt et al. (2008);

"Data were taken from Zheng et al. (2013).